Vol. 17(2), pp. 51-56, July-September, 2022
DOI: 10.5897/IJPS2022.5002
Article Number: F58C5A569696
ISSN: 1992-1950

http://www.academicjournals.org/IJPS

ACADEMIC JOURNALS
expand your knowledge

International Journal of Physical Sciences

Full Length Research Paper

Research for fabrication and antibacterial properties of hybrid nanoparticles Ag-$MnFe_2O_4$

Le Thi Thanh Tam[1] and Giap Van Cuong[2]*

[1]Vietnam Academy of Science and Technology, Institute of Materials Science, Hanoi 100000, Vietnam.
[2]Hung Yen University of Technology and Education (UTEHY), Hung Yen 160000, Vietnam.

Received 27 July, 2022; Accepted 7 September, 2022

The hybrid nanoparticles Ag-$MnFe_2O_4$ was successfully fabricated by the seed-growth method and thermal decomposition method. The shape and size of these nanoparticles were evaluated by Transmission electron microscopes (TEM) images showing that these nanoparticles are quite uniform and have a diameter of about 20 nm. The UV-Vis spectrum of hybrid nanoparticles Ag-$MnFe_2O_4$ shows that in the wavelength region from 300 to 800 nm, the ferrite manganese nanoparticle does not appear to have an absorption peak, while the spectrum of the silver nanoparticle shows a characteristic surface plasmon resonance (LSPR) peak with peaks between 400 and 420 nm. Research results show that the hybrid nanoparticles Ag-$MnFe_2O_4$ coated with PMAO (MFA10-PMAO) has the ability to inhibit both Escherichia coli bacteria-intestinal bacilli and Staphylococcus aureus bacteria. In which, the antibacterial ability with E. coli is stronger than that of S. aureus, the antibacterial zone diameter in both cases are 21.5 and 16 mm, respectively. In addition, MFA10-PMAO nanoparticles also showed easy recovery after treatment, which is favorable for reuse.

Key words: Thermal decomposition method, seed-growth method, hybrid nanoparticles Ag-$MnFe_2O_4$, Ag-$MnFe_2O_4$ nanoparticles coated with PMAO.

INTRODUCTION

The superparamagnetic properties of magnetic nanoparticles have applications in technologies such as magnetic hyperthermia, magnetic resonance imaging, contrast agents, magnetic separation, and magnetic drug delivery applications. The plasmonic properties of Ag nanoparticles have applications in technologies such as sensing, imaging and photothermal therapy. Therefore, the combination of these two materials will create new properties, multifunction, not only maximize the advantages of each material, but also limit their disadvantages when working individually. Combination of precious metal nanomaterials (Ag) and magnetic nano ($MnFe_2O_4$) in a single nanostructure that has the potential to open up new applications, such as cell extraction under plasmon-imaging, image dual mode (MRI and plasmon image), and antibacterial materials. This is possible due to hybrid structures Ag-$MnFe_2O_4$ has both the magnetic properties of manganese ferrite and the

*Corresponding author. E-mail: cuonggiapvan@gmail.com.

optical properties of the surface plasmon effect of Ag. Besides, with specific applications of each nanosystem, the idiosyncratic properties of one material can be promoted or supported by another. For example, when adding nano Ag, conductivity of $MnFe_2O_4$ improved, this hybrid structure has potential applications in storage devices, or as electrodes. In photocatalysis or wastewater treatment applications, magnetic material $MnFe_2O_4$ with heavy metal absorption and high optical conversion efficiency can help along with the bactericidal ability of Ag so that the efficiency of the process is greatly enhanced (Pankhurst et al., 2009; Hosseini et al., 2014). Besides, magnetism of $MnFe_2O_4$ makes recovery and reuse easier. General, the properties of the component materials are flexibly combined, promote and support each other when integrated on a nanoparticle. Therefore, the hybrid nanoparticle Ag-$MnFe_2O_4$ have many advantages over single nanoparticles Ag, $MnFe_2O_4$ in bioparticle separation and purification applications, enhance antibiotic activity, drug distribution, localized hyperthermia, catalysis, etc (Stafford et al., 2018; Li et al., 2018; Ning et al., 2020). Hybrid nanoparticles Ag-$MnFe_2O_4$ have been manufactured by various methods (Li et al., 2018; Bahman Mohammadian et al., 2020; Huy et al., 2017; Dong et al., 2021; Yang et al., 2021), hybrid nanoparticles Ag-$MnFe_2O_4$ in this study were successfully fabricated by the seed-growth method on the basis of $MnFe_2O_4$ particles obtained from thermal decomposition.

EXPERIMENT

Nanoparticles $MnFe_2O_4$ were prepared by thermal decomposition in organic solvents at high temperature. On the basis of fabricated manganese ferrite nanoparticles, hybrid nanoparticles Ag - $MnFe_2O_4$ were successfully fabricated by the seed-growth method.

Fabrication of hybrid nanoparticles Ag-$MnFe_2O_4$

Using 1 g silver nitrate, 6 ml Oleylamine (OLA) and 30 ml Octadecen (ODE) put them in a 3-necked flask. Continue to add 0.1 g $MnFe_2O_4$ washed and dispersed in 5 ml n-hexan. Place the three-neck flask containing the reaction mixture on the magnetic stirrer, supply nitrogen gas (Figure 1).

The reaction mixture was kept at 80°C in 30 min. Then spray quickly into a 3-necked bottle of solution containing 0.3 g OCD-ol in 10 ml ODE. Continue to increase the temperature to 200°C in 60 min. $AgNO_3$ will be reduced right on the surface of the $MnFe_2O_4$ nanoparticles form silver nanocrystals; these seeds will grow right on the surface of $MnFe_2O_4$ nanoparticles, hybrid nanoparticles Ag-$MnFe_2O_4$ were created.

Sample cleaning and preparation procedures

Samples need to be washed thoroughly before analysis to remove impurities (unreacted chemicals and byproducts of synthesis). The sample washing procedure was carried out as follows: pick 0.5 ml sample solution mixed with 0.5 ml ethanol to induce agglomeration between particles then centrifugation at speed 8000 to 12000 rpm

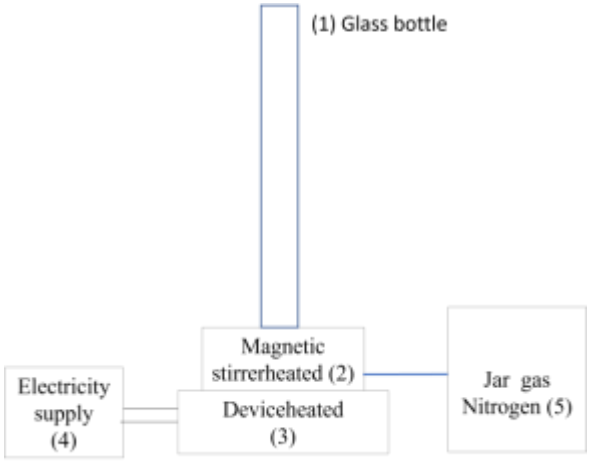

Figure 1. Pattern making diagram Ag-$MnFe_2O_4$
Source: Authors 2022

in 5 min (depending on particle size) until the particles settle to the bottom of the centrifuge tube. After removing the upper solvent, the precipitate obtained was redispersed in 0.5 ml solvent n-hexan. Sample washing is repeated 3 to 4 time, let dry naturally at room temperature.

Transferring hybrid nanoparticles Ag-$MnFe_2O_4$ in organic solvents to water

The phase transition is carried out as follows: hybrid nanoparticles Ag-$MnFe_2O_4$ cleaned according to the aforementioned washing procedure, the sample was dispersed in 1 ml chloroform, ultrasonic vibration in 3 to 5 min so that the particles are dissolved evenly. Add a quantity of poly maleic anhydride-alt-1-octadecen (PMAO) into the sample solution pre-determined has been dispersed in clorofom. Mix the aforementioned 2 solutions together and ultrasonic vibration 5 to 10 min so that the solution is mixed evenly, without sediment. The obtained product was left at room temperature for clorofom evaporate all, then add 10 ml solution NaOH diluted in water, we get samples that are capable of dispersing in water.

RESULTS AND DISCUSSION

Particle shape and size

To evaluate the formation and development of the Ag shell on the $MnFe_2O_4$ ferromagnetic core, we synthesized Ag-$MnFe_2O_4$ nanoparticles using the amount of $AgNO_3$ precursors participating in the reaction at different concentrations. Figure 2 is the TEM image of the Ag-$MnFe_2O_4$ samples showing that the obtained hybrid particles are spherical, with a core-shell structure with a $MnFe_3O_4$ core and an Ag shell. The results can be explained by the model LaMer (Chang et al., 1999; Whitehead et al., 2019; Wang et al., 2018). In the silver shell reaction, the generated Ag atoms will be deposited

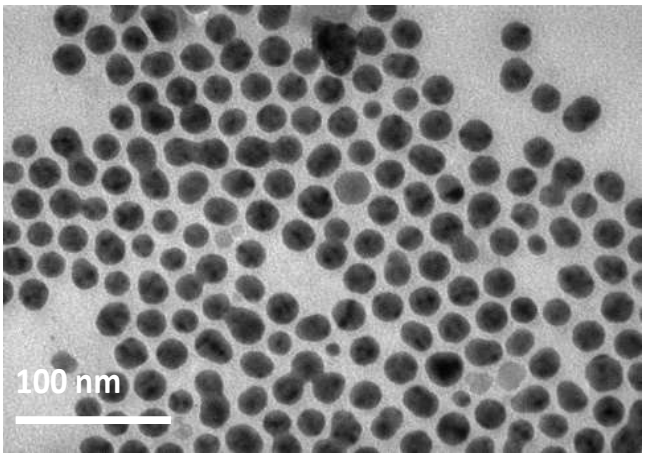

Figure 2. TEM image of hybrid nanoparticles Ag-$MnFe_2O_4$.
Source: Authors 2022

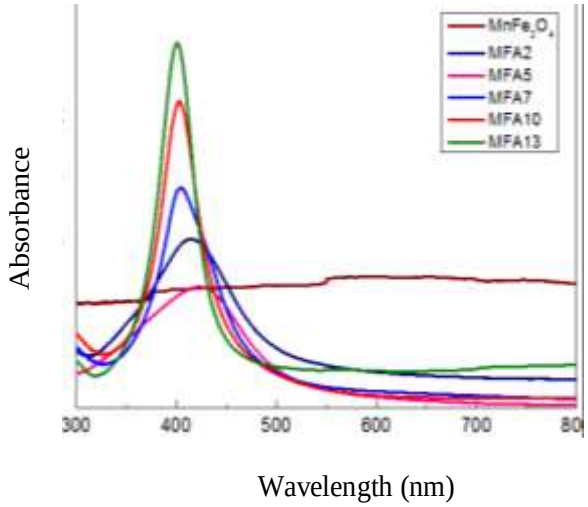

Figure 3. UV - Vis Spectrum of $MnFe_2O_4$ and Ag-$MnFe_2O_4$.
Source: Authors 2022

on the surface of the nanoparticles $MnFe_2O_4$. When on the core $MnFe_2O_4$ atoms showed Ag then those positions became active and a large amount of Ag was next deposited. Ag shells were formed continuously through the generation of Ag nanocrystals. However, when the precursor amount of Ag is low, there will be active sites with many Ag and vacancies on the core, then the Ostwald effect begins to compete and dominate over the lead deposition reaction. The process of forming the Ag shell takes place unevenly.

Optical properties

To confirm the formation of nanoparticles Ag-$MnFe_2O_4$, we measure the spectrum UV-Vis of hybrid nanoparticles Ag-$MnFe_2O_4$ fabricated and the absorption spectra of manganese ferrite nanoparticles are also shown for comparison (Figure 3). The analysis results show that in the wavelength region 300 to 800 nm nanoparticles $MnFe_2O_4$, there is no absorption peak, while the spectrum of silver nanoparticles show a characteristic surface plasmon resonance peak (LSPR), with a maximum in the interval of 400 to 420 nm. When the crust size Ag ascending from 0.9 to 5.6 nm then the surface plasmon resonance site (SPR) of hybrid nanoparticles decreased slightly from 420 to 400 nm. When the Ag shell is thin and uneven, the surface plasmon resonance peak has an expansion; when the Ag shell is thick and uniform, the surface plasmon resonance peak is narrower and more pointed as observed in Figure 3. In addition, the shape, surroundings and type of adsorption surface of the nanoparticle also affect the plasmon adsorption capacity (Anker et al., 2009; Kreuter, 2004; Walkey et al., 2012). According to Mie theory, there is only one SPR site for spherical nanoparticles (Lamer and Dinegar, 1950). Whereas anisotropic nanoparticles can appear on two or more other SPR sites, this depends on the particle shape and size.

Magnetic properties

Figure 4 shows the magnetization curves measured at room temperature of the $MnFe_2O_4$ nanoparticles and hybrid samples MFA7, MFA10 and MFA13. It can be seen that the hybrid nanopatterns Ag-$MnFe_2O_4$ all exhibit superparamagnetic properties at room temperature with MS values of 28.7, 15.9 and 9.6 emu/g, respectively for samples MFA7, MFA10 and MFA13. Saturation magnetization of the hybrid samples Ag-$MnFe_2O_4$ is much smaller than the sample $MnFe_2O_4$. This can be explained by the increase of Ag shell thickness in the core-shell structure resulting in a sharp decrease in the saturation of Ag-$MnFe_2O_4$ nanoparticles.

Although the saturation magnetic values of hybrid nanoparticles Ag-$MnFe_2O_4$ obtained are low, they can still be easily separated from solutions by applying a magnet for a few seconds.

Phase structure and composition of hybrid nanoparticle Ag-$MnFe_2O_4$

The crystal structure of Ag-$MnFe_2O_4$ hybrid nanoparticle is characterized by X-ray diffraction. As shown in Figure 5, the XRD pattern of the Ag-$MnFe_2O_4$ hybrid nanoparticle (MFA10) appears on diffraction peaks at the angular position 2θ = 38.1, 44.3 and 64.4° corresponds to the plane (111), (200) and (220) in the face-centered cubic

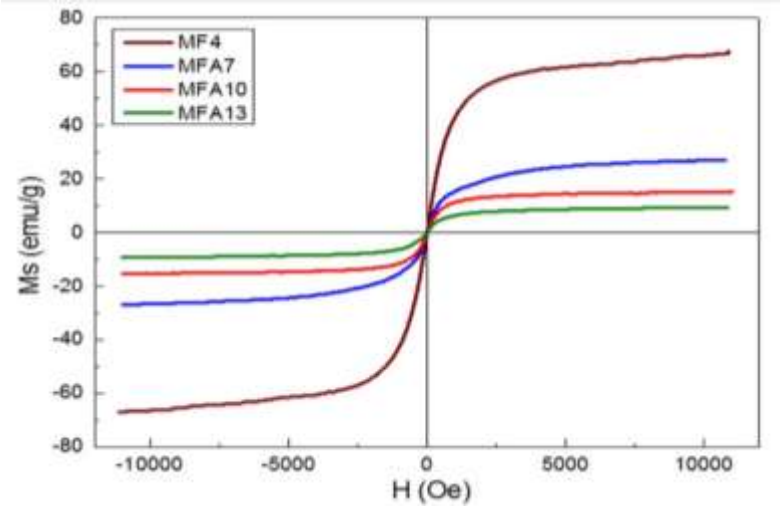

Figure 4. Magnetization curves of hybrid nanoparticles Ag-$MnFe_2O_4$.
Source: Authors 2022

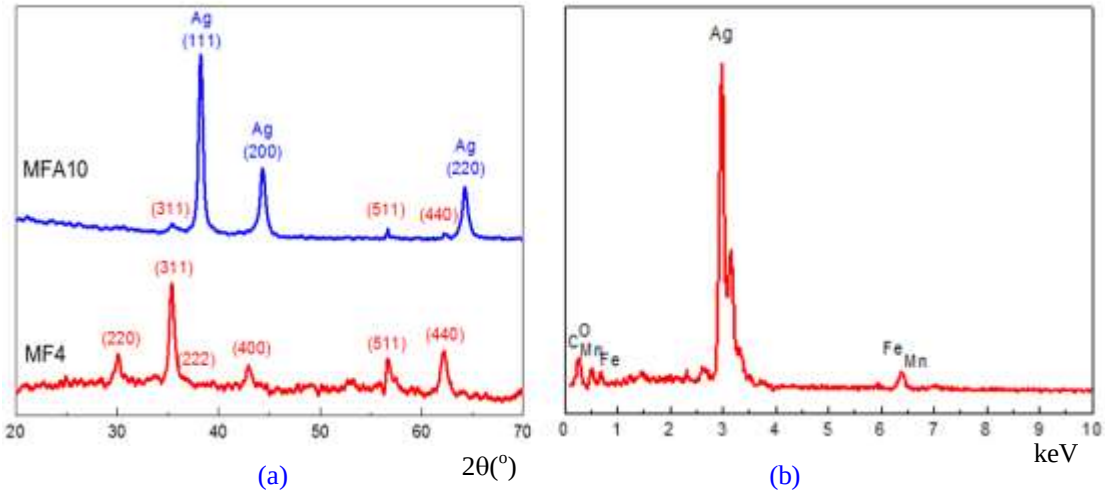

Figure 5. XRD spectrum (a) and EDX spectrum (b) of Ag-$MnFe_2O_4$.
Source: Authors 2022

structure of Ag. Besides, some peaks at position (311), (511), (440) in the spinel structure of $MnFe_2O_4$ is also observed but with very low intensity, this can be explained by the coating of the silver shell on the surface of the ferrite nanoparticle. This result is completely consistent with the results obtained from the TEM image (Figure 2). Besides, the elemental composition of Ag-$MnFe_2O_4$ hybrid nanoparticles was quantitatively analyzed by EDX scattering spectroscopy with sample MFA10, the results are presented in Figure 5.

The EDX spectrum shows that the hybrid nanoparticles consist of the main composition of Fe, Mn, O and Ag elements indicating the high purity of the sample.

To better understand the binding ability of OA, OLA and PMAO molecules on the nanoparticle surface, the FT-IR spectrum of the sample MFA10@PMAO was analyzed. Figure 6 shows that at wave number 3415 cm^{-1} assigned to OH functional group oscillations of water molecules adsorbed onto the PMAO shell of the sample, we see that the absorption peak of the sample of MFA10@PMAO is more than double that of the top of the MFA10 sample. Besides, at wave number 2853 and 2923 cm^{-1}, both samples appear absorption peak corresponding to the symmetric and asymmetric valence oscillations of CH_2 in OA, OLA and PMAO. Furthermore, the intensity of the 1570 cm^{-1} peak is significantly enhanced compared with

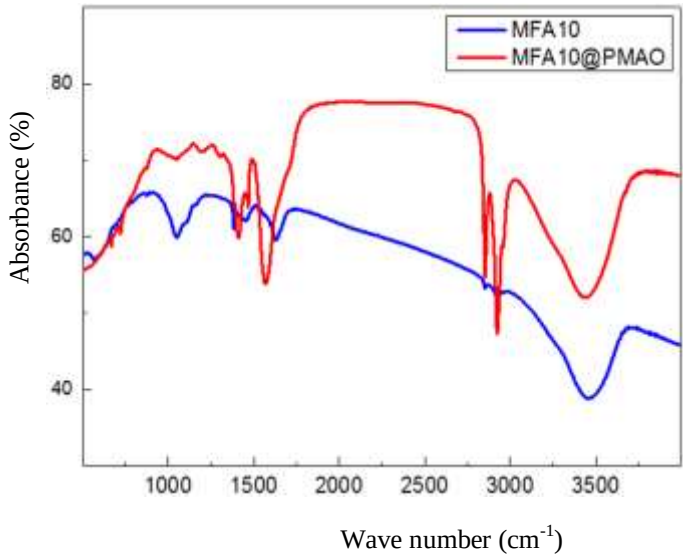

Figure 6. FTIR of MFA10@PMAO.
Source: Authors 2022

Table 1. Results of evaluation of antibacterial ability of MFA10 hybrid seeds at concentration of 0.3 mg/ml.

Type of bacteria	Antibacterial zone diameter (mm)
E. coli	21.5
S. aureus	16.0

Source: Authors 2022

the 1450 cm^{-1} peak. This result confirms that during the encapsulation of nanoparticles with PMAO, carboxylate anions are formed due to the opening of the anhydride ring.

Antibacterial ability of hybrid nanoparticle Ag-$MnFe_2O_4$

To evaluate the antibacterial ability of Ag-$MnFe_2O_4$ hybrid seeds, we performed the test in water containing pathogenic bacteria belonging to Gram-negative and Gram-positive groups with representative Gram-negative Escherichia coli (E. coli) and Gram-positive bacteria *Staphylococus aureus* with the concentration of MFA10 nanoparticles used at 0.3 mg/ml.

The evaluation results presented in Table 1 show that MFA10-PMAO hybrid seeds have the ability to inhibit both *Escherichia coli*-intestinal bacilli and *S. aureus*. In which, the antibacterial ability with *E. coli* is stronger than that of *S. aureus*, the antibacterial zone diameter in both cases are 21.5 and 16 mm, respectively. The antibacterial mechanism of Ag-$MnFe_2O_4$ hybrid nanoparticles can be explained as follows: Ag-$MnFe_3O_4$ hybrid nanoparticles, after being added to the medium containing bacteria including both Gram-negative and Gram-positive bacteria, they release linkages. Metal ions were rapidly attached to the surface of the bacterial cell wall through electrostatic interactions between the bacterial cell surface (negative charge) and Ag+ ions (positively charged). Hybrid nanoparticles dissolve the outer layer of the cell wall and lead to leakage of cellular components, enabling Ag+ to penetrate deeper into the bacterial cell to carry out reactions that generate oxygen-containing free radicals (ROS) that alter membrane permeability, interact with proteins and disrupt their function, interfere with DNA replication and damage DNA, ultimately causing cell death (Tung et al., 2016).

Conclusion

$MnFe_2O_4$ manganese ferrite nanoparticles with different morphology and sizes have been successfully

synthesized by thermal decomposition method in organic solvents at high temperature. Based on the prepared manganese ferrite nanoparticles, the hybrid nanoparticles Ag-$MnFe_2O_4$ were successfully synthesized by seed-growth method. Analyzes such as TEM, XRD, EDX, and UV-vis confirmed the formation of Ag shell on the surface of nanoparticles from manganese ferrite. The saturation of the sample after Ag coating is about 10 to 29 emu/g and still has a good magnetic response. Furthermore, this research has successfully phased Ag-$MnFe_2O_4$ hybrid nanoparticles from organic solvent to aqueous solvent by PMAO phase transition agent. These Ag-Mn_2O_4 nanoparticles have good dispersion and stability in the medium with wide pH range (pH = 2-14) and high concentration of NaCl salt (250 mM). This result shows that the PMAO coated Ag-$MnFe_2O_4$ hybrid nanoparticles respond well in terms of durability under physiological conditions.

CONFLICT OF INTERESTS

The authors have not declared any conflict of interests.

ACKNOWLEDGMENT

This research is funded by the scientific research project at Hung Yen University of Engineering and Technology under Grant No: UTEHY.L.2020.01.

REFERENCES

Anker JN, Hall WP, Lyandres O, Shah NC, Zhao J, Van Duyne RP (2009). Biosensing with plasmonic nanosensors. Nature Materials 7:442-453.

Asiabar BM, Karimi MA, Tavallali H, Rahimi-Nasrabadi M (2020). Application of $MnFe_2O_4$ and AuNPs Modified CPE as a Sensitive Flunitrazepam Electrochemical Sensor. Microchemical Journal 161:105745.

Chang SS, Shih CW, Chen CD, Lai WC, Wang CRC (1999). The Shape Transition of Gold Nanorods. Langmuir 15:701-709.

Dong H, Chen Y, Gong C, Sui L, Sun Q, Lv K, Dong L (2021). N, S, P-Codoped Graphene-Supported Ag-MnFe2O4 Heterojunction Nanoparticles as Bifunctional Oxygen Electrocatalyst with High Efficiency. Catalysts 11(12):1550.

Hosseini SH, Moghimi A, Moloudi M (2014). Magnetic, conductive, and microwave absorption properties of polythiophene nanofibers layered on $MnFe_2O_4$/Fe_3O_4 core–shell structures. Materials Science in Semiconductor Processing 24:272-277.

Huy LT, Tam LT, Van Son T, Cuong ND, Nam MH, Vinh LK, Huy TQ, Phan VN, Le AT (2017). Photochemical Decoration of Silver Nanocrystals on Magnetic $MnFe_2O_4$ Nanoparticles and Their Applications in Antibacterial Agents and SERS-Based Detection Journal of Electronic Materials 46(6):3412-3421.

Kreuter J (2004). Influence of the Surface Properties on Nanoparticle-Mediated Transport of Drugs to the Brain. Journal of Nanoscience and Nanotechnology 4(5):484-488.

Lamer VK, Dinegar RH (1950). Theory, production and mechanism of formation of monodispersed hydrosols. Journal of the American Chemistry Society 72:4847-4854.

Li Q, Zhao Y, Qu D, Wang H, Chen J, Zhou R (2018). Preparation of Ag-$MnFe_2O_4$-bentonite Magnetic Composite for Pb(II)/Cd(II) Adsorption Removal and Bacterial Inactivation in Wastewater. Chemical Research in Chinese Universities 34(5):808-816.

Ning P, Liu CC, Wang YJ, Li XZ, Ranjithkumar R, Gan ZH, Wu YY, Fua T (2020). Facile synthesis, antibacterial mechanisms and cytocompatibility of Ag–$MnFe_2O_4$ magnetic nanoparticles. Ceramics International 46(12):20105-20115.

Pankhurst QA, Thanh NTK, Dobson J (2009). Progress in applications of magnetic nanoparticles in biomedicine. Journal of physics D-applied physics 42:224001.

Stafford S, Serrano RG, Gunko Y (2018). Multimodal magnetic – Plasmonic nanoparticles for biomedical applications. Applied Sciences 8(97).

Tung LM, Cong NX, Huy LT (2016). Synthesis characterization of superparamagnetic Fe_3O_4-Ag hybrid nanoparticles and their application for hightly effective bacteria inactivation. Journal of Nanoscience and Nanotechnology 16(6): 5902-5912.

Walkey CD, Olsen JB, Guo H, Emili A, Chan WC (2012). Nanoparticle size and surface chemistry determine serum protein adsorption and macrophage uptake. Journal of the American Chemical Society 134(4):2139-2147.

Wang XG, Cheng Q, Yu Y, Zhang XZ (2018). Controlled Nucleation and Controlled Growth for Size Predicable Synthesis of Nanoscale Metal–Organic Frameworks (MOFs) A General and Scalable Approach. Internationale Ausgabe. DOI: 10.1002/anie.201803766.

Whitehead CB, Özkar S, Finke RG (2019). LaMer's 1950 Model for Particle Formation of Instantaneous Nucleation and Diffusion-Controlled Growth A Historical Look at the Model's Origins, Assumptions, Equations, and Underlying Sulfur Sol Formation Kinetics Data. Chemistry of Materials, 2019 - ACS Publications.

Yang W, Bunian M, Chen X, Heald S, Yu L, Wen J, Lei Y, Wu T (2021). Plasmon-enhanced catalytic ozonation for efficient removal of recalcitrant water pollutants. ACS ES&T Engineering 1(5):874-883.